



Article

Experimental Investigation of Two-Phase Flow Distribution with Different Vertical Header Configurations

Moojong Kim ^{1,*}, Mark Anthony Redo ², Jongsoo Jeong ¹, Kiyoshi Saito ³, Sangmu Lee ⁴ and Hyunyoung Kim ⁴¹ Research Institute for Science and Engineering, Waseda University, Shinjuku-ku, Tokyo 169-8555, Japan² Department of Food Science and Technology, Tokyo University of Marine Science and Technology, Minato-ku, Tokyo 108-8477, Japan³ Department of Applied Mechanics and Aerospace Engineering, Waseda University, 3-4-1 Okubo, Shinjuku-ku, Tokyo 169-8555, Japan⁴ Samsung Research and Development Institute Japan, Osaka 562-0036, Japan

* Correspondence: mj_kim@aoni.waseda.jp

Abstract: In this study, we investigated the behavior of two-phase flow distribution inside a vertical header of a microchannel heat exchanger (MCHX) that functions as an evaporator of a heat pump system. In general, the two-phase flow distribution behavior of the refrigerant differs depending on the target application, which ranges from small-scale automobile air-conditioners to large-scale building heat pump systems. Particularly, it is reported that the distribution characteristics in the vertical header of the MCHX vary extensively according to the inlet flow conditions of the refrigerant and the physical profile of the header. In this study, the physical configurations (header height, branch tube diameter) of four types of vertical headers were considered. Thereafter, the operating conditions in an experimental device that simulates an MCHX with a vertical header were selected. The experiment was performed under R410A as the working fluid, with a saturation temperature of 15 °C, inlet mass flow rate of 50–150 kg h⁻¹ (mass flux of 908–2723 kg m⁻² s⁻¹), and an inlet vapor quality of 0.1–0.2. The liquid and vapor flow ratios and the relative standard deviation were adopted as metrics to characterize the uniformity of flow distribution. The distribution characteristics were subsequently described according to Reynolds and Froude numbers. The larger the Reynolds number and the smaller the Froude number, the more uniform the two-phase flow distribution becomes. A correlation was proposed as a function of the Reynolds and Froude numbers to predict the flow distribution characteristics for the considered vertical headers.

Keywords: heat pump; microchannel heat exchanger; flow distribution; vertical header; header structure; maldistribution



Citation: Kim, M.; Redo, M.A.; Jeong, J.; Saito, K.; Lee, S.; Kim, H. Experimental Investigation of Two-Phase Flow Distribution with Different Vertical Header Configurations. *Energies* **2022**, *15*, 8320. <https://doi.org/10.3390/en15218320>

Academic Editors: Hussein A. Mohammed and Adrián Mota Babiloni

Received: 12 September 2022

Accepted: 30 October 2022

Published: 7 November 2022

Publisher's Note: MDPI stays neutral with regard to jurisdictional claims in published maps and institutional affiliations.



Copyright: © 2022 by the authors. Licensee MDPI, Basel, Switzerland. This article is an open access article distributed under the terms and conditions of the Creative Commons Attribution (CC BY) license (<https://creativecommons.org/licenses/by/4.0/>).

1. Introduction

An MCHX is a type of heat exchanger that has been rapidly developed in recent years [1,2]. Compared to traditional heat exchangers, MCHX offers certain advantages: downsizing (consuming less space) and requiring less refrigerant in the system [3]. These features and low-cost manufacturing techniques with material savings lead to a competitive manufacturing process compared to fin-tube heat exchangers [4–6]. MCHXs have great potential to address the demand for small and lightweight heat exchangers that can be used in small-to-large-size HVAC systems and refrigeration applications, such as for aviation, automotive, electronic equipment, chemical, industrial, commercial, and residential systems [7]. Compared to the conventional heat exchanger, MCHX has a small hydraulic diameter of less than 1 mm, and the reduced cross-sectional area result in a relatively high-pressure drop [8,9]. However, this high-pressure drop is maintained at an acceptable level by applying a common header (also called a manifold) and using parallel tubes that branched out from the header.

An MCHX with a vertical header typically functions as an evaporator in a heat pump cycle. The two-phase refrigerant flows into the evaporator with an inlet quality of about 0.1 to 0.2 and then separates into liquid and vapor phases as it enters the header. In the two-phase flow, a difference in property parameters such as density, velocity, and buoyancy of the fluid occurs for each phase, further causing a nonuniform flow distribution. As a result, dry-out occurs in some branched microchannel tubes, which leads to reduced heat transfer efficiency and affects the overall system performance [10]. It should be noted that the dry-out inside the evaporator is not simply a matter of efficiency reduction. The absence of liquid inside the evaporator promotes oxidation owing to the rapid temperature rise and causes a local melting point [11]. This phenomenon may appear differently depending on the working fluid, operating conditions, and shape of the heat exchanger [12–14]; however, this ultimately causes heat exchanger failure. This problem can be solved by improving the flow distribution within the header through an optimal design of the header.

In the studies of Amador [15], Kandlikar et al. [16], and Cho et al. [17], the analyses of the flow distribution inside the header were conducted by focusing on the single-phase flow. It was found that the pressure drop due to the friction inside the tube has a significant influence on the flow distribution. However, it should be noted that the two-phase flow distribution through the manifold is a complex phenomenon, and the main factors are diverse. Among various factors, it is well-known that the structural and geometrical design of the heat exchanger, operating conditions (mass velocity, inlet quality, flow pattern, and heat load), and properties of the working fluid are affected [18–20].

Regarding the header geometry, Siddiqui and Zubair [21] studied various design factors affecting the flow distribution of the heat exchanger. This comprehensive review demonstrates that the design of the header layout and dimensions is an essential factor for uniform flow distribution. Lee [22] investigated the two-phase flow distribution inside the vertical header of a compact heat exchanger with parallel channels. It was confirmed that the recirculation of the two-phase upstream of the vertical header is also significant in the flow distribution.

Regarding the operating conditions, the study of Hwang et al. [23] examined the influence of various operating conditions on the flow distribution in a heat exchanger with a horizontal header. This research confirmed that the effects of the mass flow rate and inlet vapor quality were more significant than those of the heat load. Redo et al. [24] investigated the two-phase flow distribution according to changes in the mass flow rate and inlet quality for vertical headers with parallel microchannels. This study confirmed a relatively uniform distribution at a higher mass flow rate and a lower inlet quality. As revealed from the studies of Fei and Hrnjak [25] and Ahmad [26], the flow pattern can also be considered a significant factor of flow distribution, which is an essential parameter in horizontal headers rather than in vertical headers.

As in the studies described above, the two-phase flow distribution in the header has been investigated using different parameters from various viewpoints. In particular, the available works on vertical headers with horizontal microchannels, which is the subject of this study, have mainly considered compact heat exchangers with low mass flow rates and are focused on automotive air conditioning applications. These sizes and ranges are insufficient to consider the actual operating conditions of residential or commercial air conditioners. Moreover, the flow distribution in the vertical header must consider the effect of the height because the influence of gravity is relatively emphasized [27]. The vertical header of a residential air conditioner is approximately 500 mm; under such conditions, the flow distribution imbalance could be further aggravated.

As explained above, from the viewpoint of a vertical header design, the improvement of two-phase flow distribution to prevent dry-out is very important. In this study, two types of vertical headers were considered to investigate the effect of the header heights: one with a height of 490 mm for simulating a heat pump system and another with a height of 190 mm for simulating a compact heat exchanger. To focus on the effect of the variation in header height, the parallel tubes were considered as simplified 3 mm smooth tubes

with a pressure control valve. In addition, two sets of header outlet inner diameters were considered to intentionally control the distribution resistance. A small cross-sectional area of 15.30 mm² was considered to provide a sufficient inertial force in the tall height case. The effect of the high Reynolds number on the two-phase flow distribution was compared with that of the conventional vertical header. For operating conditions, a mass flow rate of 50–150 kg h⁻¹ (mass flux of 908–2723 kg m⁻² s⁻¹) and an inlet vapor quality of 0.1–0.2 were considered. In particular, the analysis of the two-phase flow distribution behavior according to the change in hydrodynamic parameters can be an essential indicator for suggesting the direction of the actual design. For this, an empirical correlation expressed by the Reynolds and Froude numbers has also been proposed.

2. Experimental Investigation

2.1. Experimental Apparatus

Figure 1 shows a schematic of the experimental apparatus used to measure the flow distribution. The refrigerant loop was made of a copper tube with an inner diameter of 7.1 mm; the loop flowed from the receiver tank to the preheater through the sub-cooler using a magnetic geared pump (MML series; Sanwa Corp.: Suita, Osaka, Japan) to prevent oil mixing and pulsation. The refrigerant in the subcooled state was heated by the preheater and converted to a two-phase state with a specific inlet vapor quality. The two-phase refrigerant flows into the test section, from the front header to the rear header, and returns to the receiver tank after the condensation. To reduce heat loss to the room environment, the entire component of the apparatus was insulated using a 10-mm-thick Aeroflex insulation. The inlet flow rate of the refrigerant that enters the header was controlled by adjusting the revolutions per minute of the magnetic geared pump and was measured using a liquid Coriolis flow meter (ALTI mass II type U; Oval: Shinjuku, Tokyo, Japan) with an accuracy of ±0.05%. For a precise measurement of the individual flow rate of each tube, the individual refrigerant flow was converted to a superheated gas state at the bypass line of the test section before it entered the vapor Coriolis flow meter (ALTI mass II type U; Oval: Shinjuku, Tokyo, Japan). The heat input was controlled through an electric heater with a capacity of 3 kW. At this time, the power consumption of the heater was measured in the same manner as that of the preheater. The inlet vapor quality was adjusted using an electric preheater with a capacity of 6 kW, and the heater's power consumption was measured using a power analyzer (PW3336; Hioki Corp.: Ueda, Nagano, Japan) with ±0.15% accuracy. The pressure and temperature in the test section (from front to rear headers) were controlled by a separate external temperature control system to regulate the cooling capacity of the condenser. The pressure of each section was measured using a pressure transducer (FP101A; Yokogawa Electric Corp.: Musashino, Tokyo, Japan) with ±0.25% full-scale accuracy, and the temperature was measured using a PT100 RTD sensor (Class A, Sakaguchi Bunkado Co., Ltd.: Kadoma, Osaka, Japan) with ±0.15 °C accuracy. The uncertainty for the inlet vapor quality was ±5.17% ($x = 0.2, 15\text{ °C}, 100\text{ kg h}^{-1}$).

Using the experimental device described above, three flow rate conditions (50, 100, and 150 kg h⁻¹; with a corresponding mass flux of 908, 1815, and 2723 kg m⁻² s⁻¹), and two inlet quality conditions (0.1, 0.2), were selected by considering the operating conditions of the actual evaporator of the residential heat pump system. The saturation temperature and pressure were set to 15 °C and 1.2584 MPa, respectively. Furthermore, the refrigerant used was R410A. Table 1 summarizes the experimental conditions used in this study.

Table 1. Summary of experimental inlet conditions.

Variable	Conditions
Mass flow rate, \dot{m} (kg h ⁻¹)	50, 100, 150
Mass flux, G (kg m ⁻² s ⁻¹)	908, 1815, 2723
Inlet vapor quality, x	0.1, 0.2
Saturation temperature, T_{sat} (°C)	15

Table 1. Cont.

Variable	Conditions
Saturation pressure, P_{sat} (MPa)	1.2854
Refrigerant	R410A

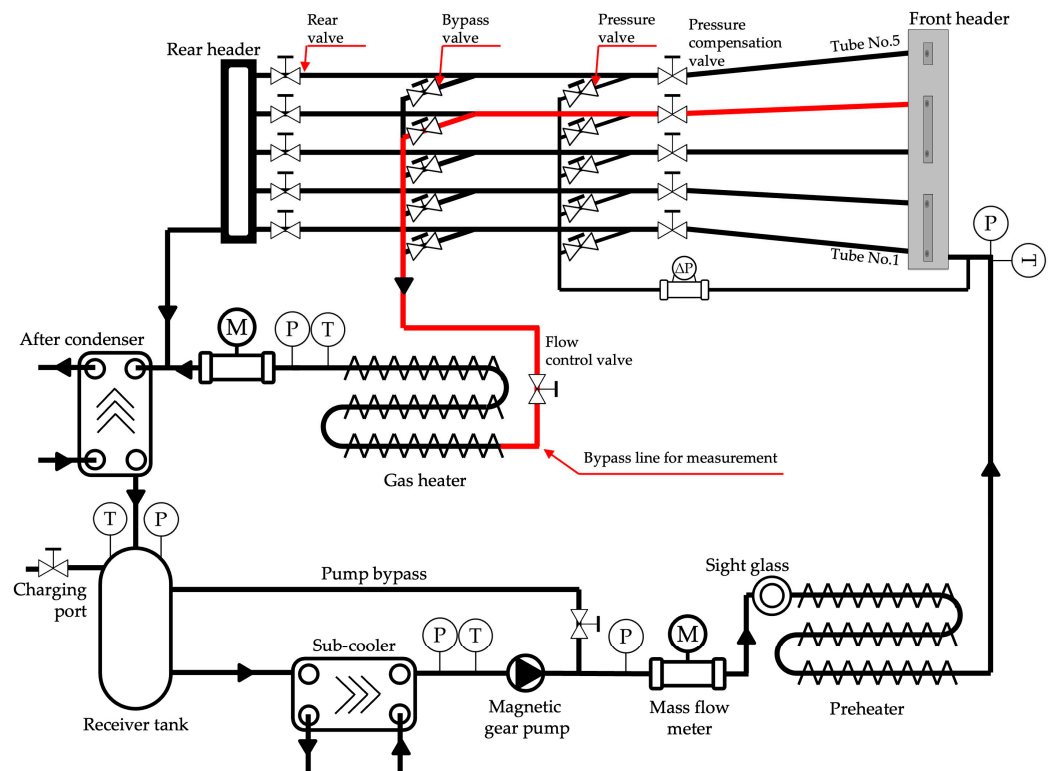


Figure 1. Schematic diagram of the experimental apparatus.

2.2. Test Section

This study considered four original vertical headers to analyze the effects of inertia and gravitational forces on the flow distribution based on the above-mentioned previous studies. Figure 2 depicts four types of vertical headers. All headers consist of a trapezoidal inner cross-section. A cross-sectional area of 15.3 mm^2 was preliminarily chosen as a possible solution to boost the liquid flow [28]. Owing to the small cross-sectional area, the mass flux range inside the header was approximately $908\text{--}2723 \text{ kg m}^{-2} \text{ s}^{-1}$.

The height of the vertical header was considered in two cases: 120 mm (Figure 2a,b) and 420 mm (Figure 2c,d), from the first tube (tube number 1) to the last tube in the flow direction. In the case of 120 mm, the size represents the vertical header of a compact heat exchanger, while in the case of 420 mm, the vertical header of the heat exchanger of an actual air conditioner was considered. The height from the entrance of the vertical header to the first tube was 70 mm for both headers. Five tubes branched out from the vertical header. Here, two header outlet inner diameter sets were considered to control the distribution resistance: the same-diameter set (header sets 1 and 3) and the different-diameter set (header sets 2 and 4). The same-diameter set was designed to simulate a microchannel heat exchanger with common parallel branches and had an inner diameter of 2.3 mm in all header outlets. The different-diameter set was designed to compensate for the lack of flow distribution at the top of the vertical header in the flow direction (tube number 5) considered in previous studies [24], where the header outlet gradually increases in the inner diameter from tubes 1 to 5. The details of the four header sets considered in this study are listed in Table 2.

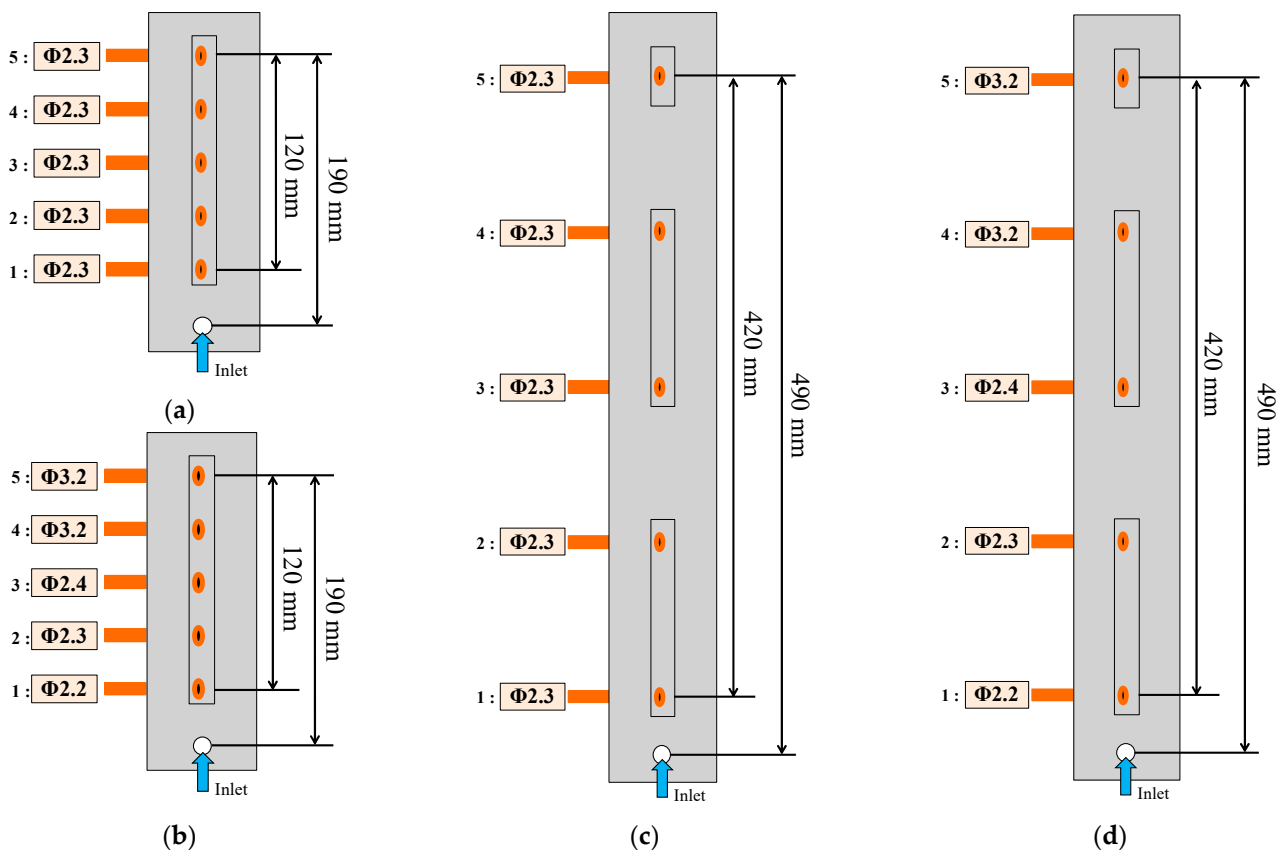


Figure 2. Four types of originally designed vertical headers: (a) header set 1; (b) header set 2; (c) header set 3; (d) header set 4.

Table 2. Details of the four header sets.

	Header Set 1	Header Set 2	Header Set 3	Header Set 4
Total height (mm)	190	190	490	490
Inlet to first tube height (mm)	70	70	70	70
Tube interval (mm)	30	30	105	105
Header outlet diameter set	same	different	same	different

To measure the flow distribution of vertical headers of various sizes using a single experimental facility, the branch tubes from the vertical header were replaced with five smooth circular tubes, which simulated parallel-branching microchannels. However, owing to the difference in the height of each vertical header, branched tubes were installed at an inclination angle. The inclination angle of a 120 mm header diverged from the header, and that of a 420 mm header converged from the header. Figure 3 depicts an example of the installation of a 120 mm header.

Due to this limitation of installation, in the 120 mm header, the flow in the first tube (tube number 1) in the flow direction undergoes acceleration due to gravity, and the flow in the last tube (tube number 5) undergoes deceleration due to gravity. This imbalance of acceleration and deceleration affects the flow distribution in the header; hence, compensation is required. Compensation is performed through the pressure compensation valve located on the downstream side, as shown in Figure 3. For example, the same flow rate of fluid in the tube under single-phase flow can be considered. The pressure drop of the fluid inside the first tube (tube number 1) of the 120 mm header is reduced compared to that of the non-inclined tube due to the inclination angle. Conversely, the pressure drop in the last tube (tube number 5) of the 120 mm header increased compared to the non-inclined tube. This acceleration/deceleration trend is reversed in the 420 mm header, and the

pressure drop of each tube in the single-phase experiment of each header is adjusted and compensated so that it has the same value using the pressure control valve.

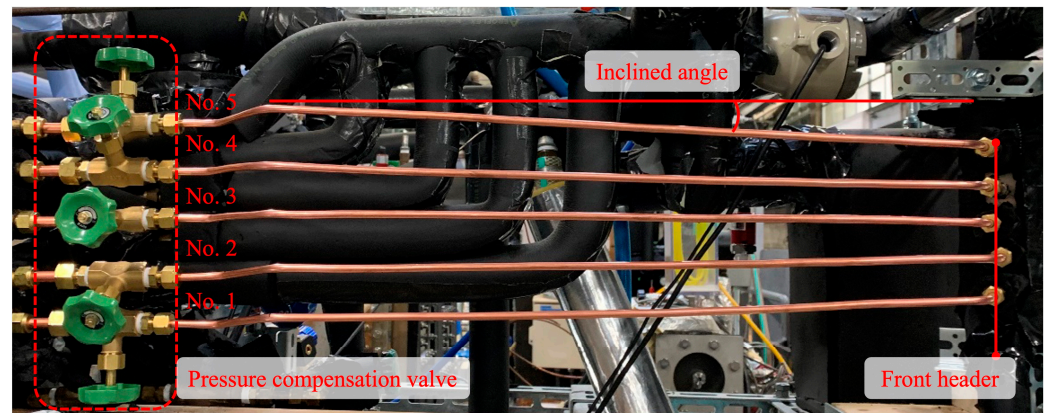


Figure 3. Example of the installation of a 120 mm header.

2.3. Measurement Procedure

To analyze the flow distribution of the vertical header, it is essential to measure the individual flow rate and quality for each tube. Both values (flow rate and vapor quality) for each tube were measured in the bypass line. The following procedure was carried out to accurately measure the individual flow rate and vapor quality for each tube.

After reaching a steady state in the experimental condition, the pressure drop for each tube was measured by opening the corresponding pressure valve. These pressure drops were considered as the reference pressure drop for measuring the individual flow rate. Thereafter, the bypass valve of the tube was opened, and the rear valve located in front of the rear header was closed. To measure the individual mass flow rate and quality, the flow path was changed to the bypass line. As an illustrative example shown in Figure 1, the flow path in tube number 4, which passes through the bypass line for measurement, is highlighted in red line.

It should be noted that a single-phase flow is required to precisely measure the individual flow rate. For this purpose, the two-phase fluid was converted into a single-phase flow in a superheated state through a heater located in the bypass line. The power consumption (Q_s) of the heater was measured using the power analyzer necessary for the data reduction of individual quality. Simultaneously, the pressure loss in the current tube was adjusted to obtain the same value as the reference pressure pressure loss by regulating the flow control valve in front of the gas heater. This procedure allows the individual flow rate and quality to be measured for all experimental conditions while maintaining the superheated state. This procedure was repeated for all the branched tubes. The uncertainty of individual vapor quality was 8.42%.

2.4. Data Reduction and Evaluation Parameters

The inlet vapor quality of the header ($x_{h,in}$) is expressed by Equation (1),

$$x_{h,in} = \frac{i_{h,in} - i_f|_{T_{h,in}}}{i_{fg}|_{T_{h,in}}} \quad (1)$$

where $i_f|_{T_{h,in}}$ and $i_{fg}|_{T_{h,in}}$ are the saturated liquid specific enthalpy and specific latent enthalpy of the vertical header, respectively. Here, $i_{h,in}$ is the specific enthalpy of the two-phase flow at the entrance of the vertical header. It can be calculated using Equation (2),

$$i_{h,in} = i_{ph,in} + \frac{Q_{ph}}{\dot{m}} \quad (2)$$

where $i_{ph,in}$ is the specific enthalpy of the subcooled liquid refrigerant at the inlet of the preheater, and Q_{ph} is the amount of measured power consumed by the preheater.

The individual quality (x_i) of the two-phase flow branched into each tube can be calculated using Equation (3),

$$x_i = \frac{\dot{m}_i (i_{bp,s} - i_f|_{T_i}) - Q_s}{\dot{m}_i i_{fg}|_{T_{h,in}}} \quad (3)$$

where \dot{m}_i is the individual flow rate of each tube measured in the bypass line and $i_{bp,s}$ is the enthalpy derived from the temperature (T_s) and pressure (P_s) of the superheated gas-phase refrigerant flow in the bypass line. Q_s is the amount of measured power consumed by the preheater.

Subsequently, $\dot{m}_{l,i}$ and $\dot{m}_{v,i}$ can be derived from the relationship between each phase's quality and individual flow rate, as shown in Equation (4) and (5).

$$\dot{m}_{l,i} = \dot{m}_i(1 - x_i) \quad (4)$$

$$\dot{m}_{v,i} = \dot{m}_i x_i \quad (5)$$

From $\dot{m}_{l,i}$ and $\dot{m}_{v,i}$, the flow ratio of each phase of the two-phase flow inside each tube can be defined using Equation (6) and (7).

$$FR_{l,i} = \frac{\dot{m}_{l,i}}{\sum \dot{m}_{l,i}} \quad (6)$$

$$FR_{v,i} = \frac{\dot{m}_{v,i}}{\sum \dot{m}_{v,i}} \quad (7)$$

The flow ratio is the distributed vapor/liquid flow rate of each tube compared to the inlet vapor/liquid flow rate. The sum is one, which is constant in all cases and can be used as an evaluation parameter of the flow concentration.

The relative standard deviation (RSD) was considered as another evaluation parameter [28,29]. In statistics, the RSD is usually a standardized measure of the deviation of a set of numbers, calculated as the ratio of the standard deviation to the mean. It has a value between zero to one, with values closer to one indicating that each element of a set of numbers is far from the average value and closer to zero indicating closer to the average value [30]. As shown in Equation (8), RSD is used to compare the measurement results of this study targeting various flow rates and inlet quality. Under all conditions, the closer the RSD value is to zero, the more uniform the flow distribution is.

$$RSD = \frac{\sqrt{\frac{1}{n} \sum_1^n (\dot{m}_{j,i} - \dot{m}_{avg,j})^2}}{\dot{m}_{avg,j}} \quad (8)$$

3. Results and Discussion

This section compares and analyzes the flow distribution results for various inlet conditions for the four header configurations. Subsequently, a new correlation for the considered type of header has been proposed.

3.1. Flow Distribution Profile for Each Phase

Figures 4 and 5 depict the liquid and vapor flow ratios based on the system flow rate and header inlet quality for the four header sets. The liquid and vapor flow ratios in each

tube are shown to present the overall experimental results briefly and comprehensively. The upper sections of Figures 4 and 5 show the results for the 190 mm headers (header sets 1, 2), and the results for the 490 mm headers (header sets 3, 4) are depicted at the bottom. The header considered in this study has a higher Reynolds number than that considered in a previously reported study. Therefore, unlike the observations in previous studies, the liquid flow distribution is concentrated at the top, and the vapor flow distribution is mostly at the bottom.

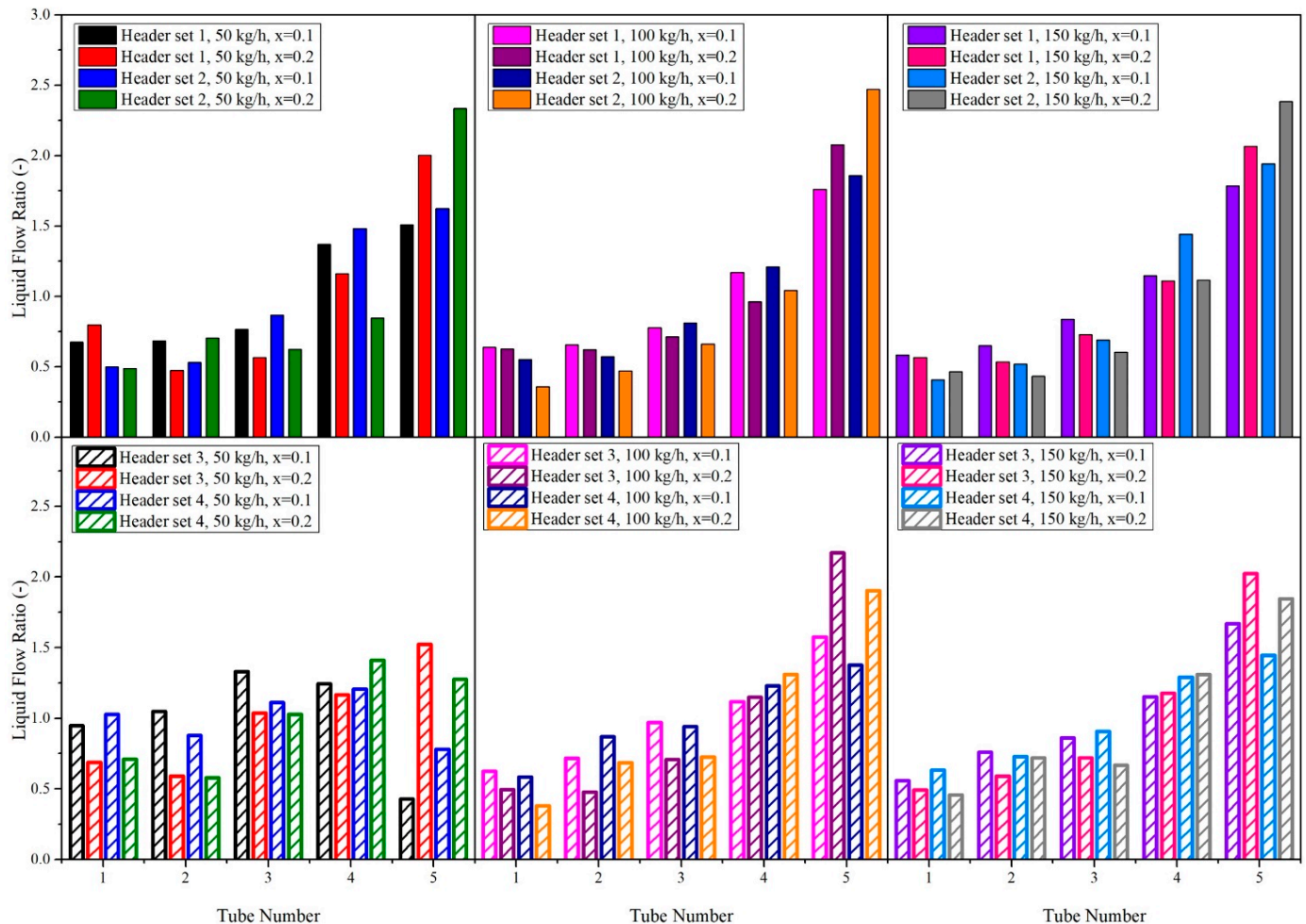


Figure 4. Liquid flow ratio of the four vertical headers.

3.1.1. Liquid-Phase Distribution

As depicted in Figure 4, for most cases, the liquid flow ratio increases in the top tube (tube number 5) regardless of the header inlet conditions (flow rate and quality). In the case of header sets 3 and 4 at 50 kg h^{-1} , the relatively small inlet flow rate prevents a significant amount of liquid from reaching the top tube. As described above, an increase of the flow ratio in a specific tube means that the corresponding tube's fluid (liquid, vapor phase) flow rate is relatively higher than that of the other tubes. This trend is exacerbated as the system flow rate increases and the header inlet quality increases. Moreover, this trend becomes more apparent in the different header outlet inner diameter sets (header sets 2 and 4). In particular, the increase in the inlet quality significantly aggravated the nonuniformity of the liquid-phase distribution. However, as the height of the header increases (from 190 mm to 490 mm), the flow distribution becomes relatively uniform.

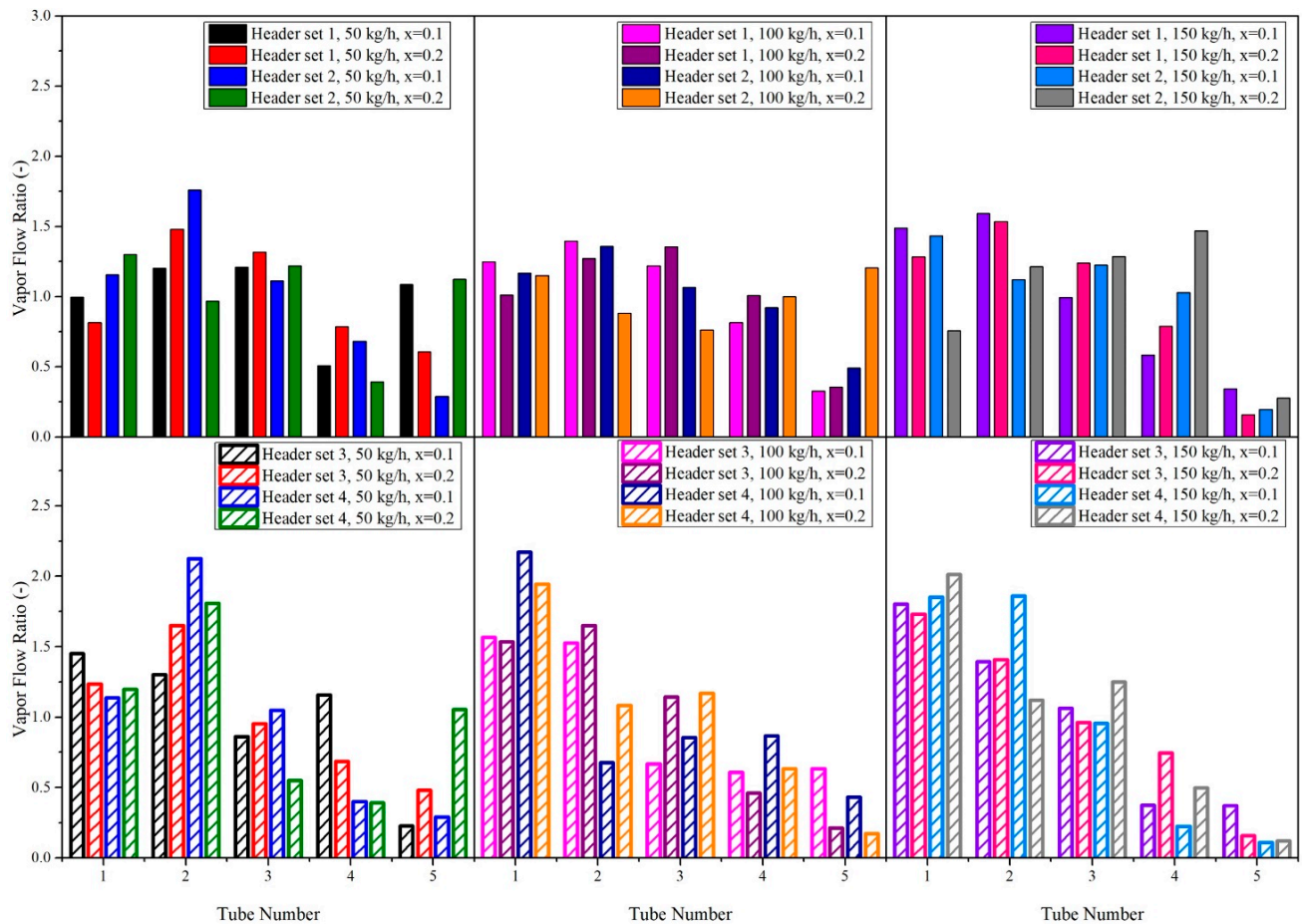


Figure 5. Vapor flow ratio of the four vertical headers.

3.1.2. Vapor-Phase Distribution

As depicted in Figure 5, the vapor flow ratio in the lower tubes is considerably higher than that in the upper tubes, which means that the vapor flow is relatively concentrated in the lower tubes. In the case of a 190 mm header, the flow ratio at the lower tubes is less than in the case of a 490 mm header. The trend is perhaps due to the inertial force being more dominant than the gravitational force. The height of the header promotes vapor supply to the upper region in the case of a 190 mm header. Oppositely, in the case of the 420 mm header set, gravity has more influence than inertia, which leads to intensified nonuniform vapor flow distribution. For all header sets, the nonuniformity increases with the system flow rate and with the different outlet inner diameter sets (header sets 2 and 4). However, in most cases, an increase in the inlet quality reduces the nonuniformity.

3.2. Relative Standard Deviation

The flow distribution results according to the change in the inlet conditions for the four types of header sets can be shown more intuitively through the relative standard deviation (RSD) results. Figure 6 depicts the RSD results for all the experimental conditions. Through this, it can be noted that the liquid and vapor flow ratios have opposite trends according to the header set and inlet quality, regardless of the header inlet flow rate. A low liquid flow RSD case indicates a high vapor flow RSD. The liquid flow has the minimum value of RSD (0.17) in the header set 4 (490 mm header) with different outlet inner diameter sets. Furthermore, in the case of the vapor phase, it shows the minimum RSD value (0.18) in the header set 2 (190 mm header) with different outlet inner diameter sets. However, the minimum RSD of each phase for the entire experimental case was observed at different flow rate conditions. These results show that the rational flow distribution can be derived

according to the various geometrical parameters (cross-sectional area, height, and outlet inner diameter of a header) and the system's working conditions (flow rate and inlet vapor quality). It is also expected that the flow distribution can be controlled by combining these parameters and conditions.

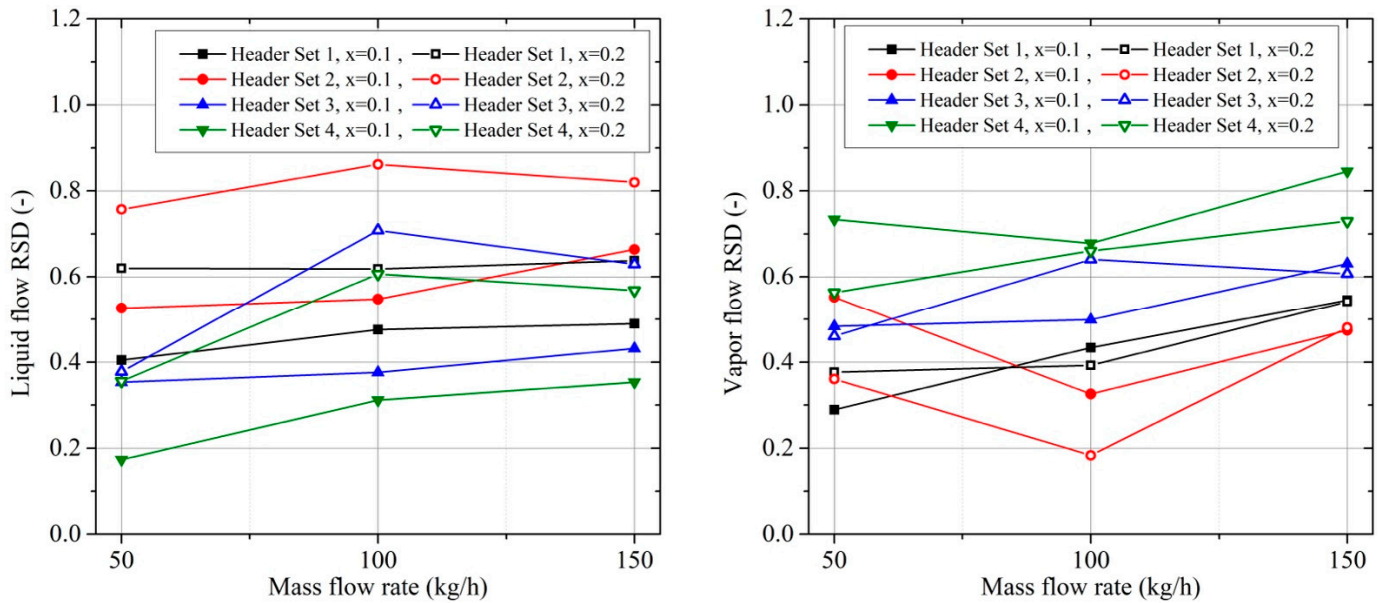


Figure 6. Relative standard deviation for the four vertical headers.

3.3. Effect of Different Parameters on Flow Distribution

In this section, the effect of varying the operating conditions and structural parameters on flow distribution was further explored. For the flow rate, an increase in flow generally promotes liquid inflow and decrease of vapor inflow to the upper section. This phenomenon is typical to separated two-phase flow in vertical headers, which transports maldistribution (increased RSD) of the liquid and vapor flow as the flow rate increases.

However, it is complicated to analyze the effect of parameter changes unless represented by the flow rate. Therefore, the flow distribution profiles in Figures 4 and 5 were rearranged to produce Figures 7–9 to highlight the analysis of the target parameter. The figures are divided into sub-figures for an easy but comprehensive comparison of the results, with the inclusions of RSD to aid the quantitative liquid and vapor flow distribution evaluation. The structural details for each header set are summarized in Table 2.

3.3.1. Effect of Inlet Vapor Quality

Figure 7 shows the flow distribution profiles according to the change in inlet vapor quality. The results of header sets 1 and 3 with the same header outlet tube diameter are presented. As the inlet quality increases, the liquid flow ratio at the upper section (tube numbers 4 and 5) generally increases. In the case of 50 kg h^{-1} in the header set 3, a low liquid flow ratio was observed in tube number 5 due to the increased height of 490 mm. In the same header set, it is observed that the liquid flow ratio increases as the inlet quality increases. The increment in inlet quality induces the concentration of liquid flow to the upper section of the header, owing to the rise in inertial force and an increase in gas-phase flow rate. Therefore, the vapor flow traversing into the upper section also rises in the direction of tube number 5, which can be recognized by the rise of the vapor flow distribution's peak position (red arrow).

However, the introduction of an additional inertial force from the increase of the gas-phase flow rate promotes the liquid inflow into the upper section, which leads to the liquid distribution degradation, indicated by the liquid flow RSD increment as the inlet quality increases.

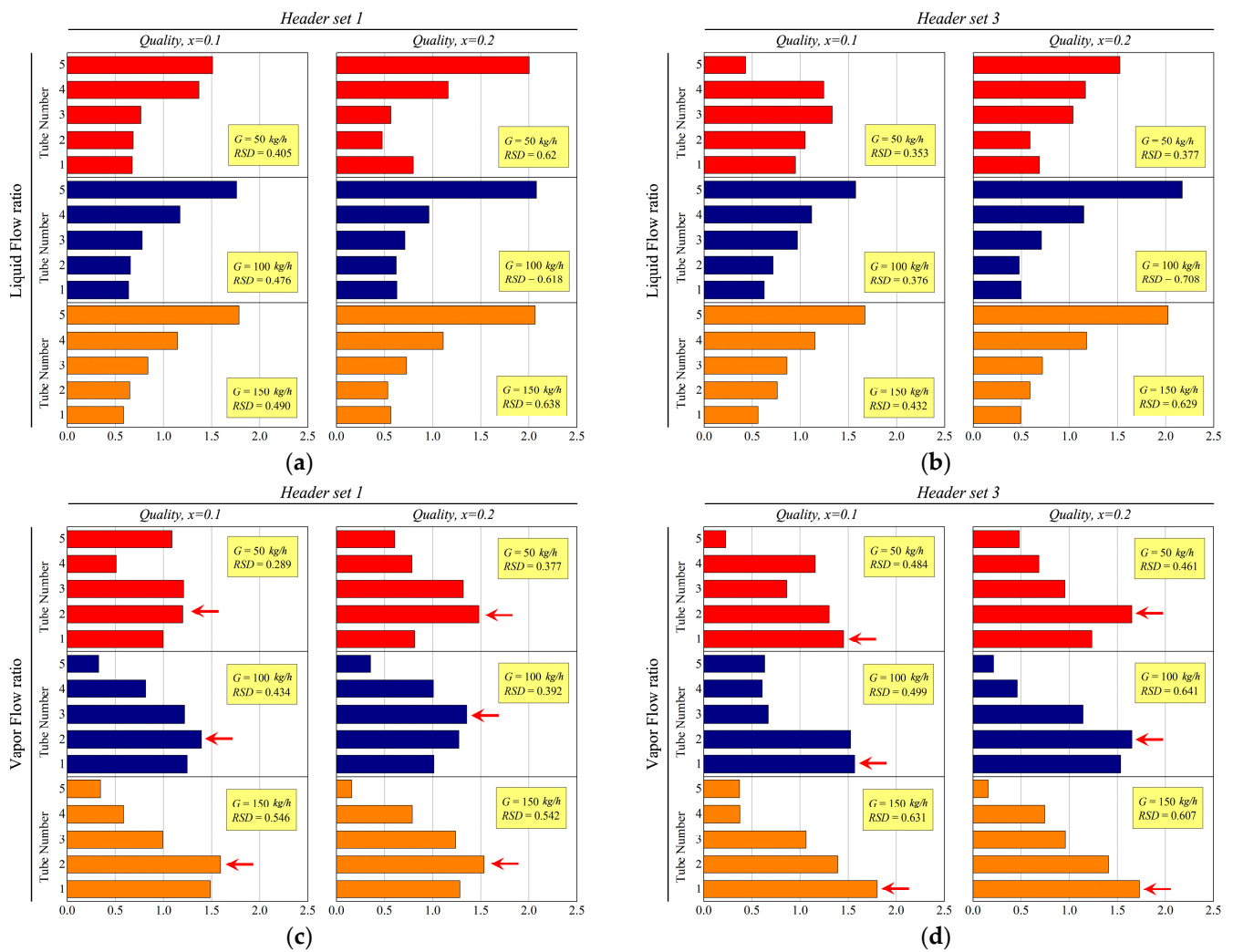


Figure 7. Effect of inlet quality to flow distribution profile: (a) liquid flow ratio, the header set 1 (190 mm); (b) liquid flow ratio, the header set 3 (490 mm); (c) vapor flow ratio, the header set 1 (190 mm); (d) vapor flow ratio, the header set 3 (490 mm).

3.3.2. Effect of Header Outlet Tube Diameter

Figure 8 shows the flow distribution profiles at $x = 0.1$ according to the variation of the header outlet tube diameter set. The headers with the same height were grouped and compared. While header sets 1 and 3 comprise of fixed outlet tube diameter, header sets 2 and 4 feature an increasing tube diameter size towards the upper section, as shown in Figure 2. For the short headers (190 mm), the liquid flow rate that exits at the upper section is greater for header set 2 (different outlet tube diameter) than in header set 1 (same outlet tube diameter). Because the former has a larger diameter at the upper section, it is thought that the liquid flow is enhanced in this region as the resistance to the fluid is reduced. Here, the increase of liquid inflow according to the change in the outlet tube diameter is smaller than the increase of the inlet quality (represented in Figure 7), which means that the rise in inertial force according to the change in the outlet tube diameter is relatively smaller than the effect of the inlet quality.

On the other hand, for the tall headers (490 mm), a better liquid flow distribution is obtained in header set 4 (different outlet diameter), especially at an inlet mass flow rate of 50 kg h^{-1} compared with that in the header set 3 (same outlet diameter). A slight inflow increase into tube numbers 3 and 4 is observed, perhaps due to a relatively small increase in inertial force, as previously mentioned. That is, if the height of the header changes, the influence of the inertial force also changes. In the vapor flow distribution, only a slight

change is observed due to a relatively small increase in inertial force, which is more evident in the short header.

As described above, unlike the increase of the inlet quality, the effect of promoting liquid flow into the upper section from different outlet diameter sets is different depending on the height, so it can be confirmed that the RSD increases in the short headers, while it decreases in the tall headers.

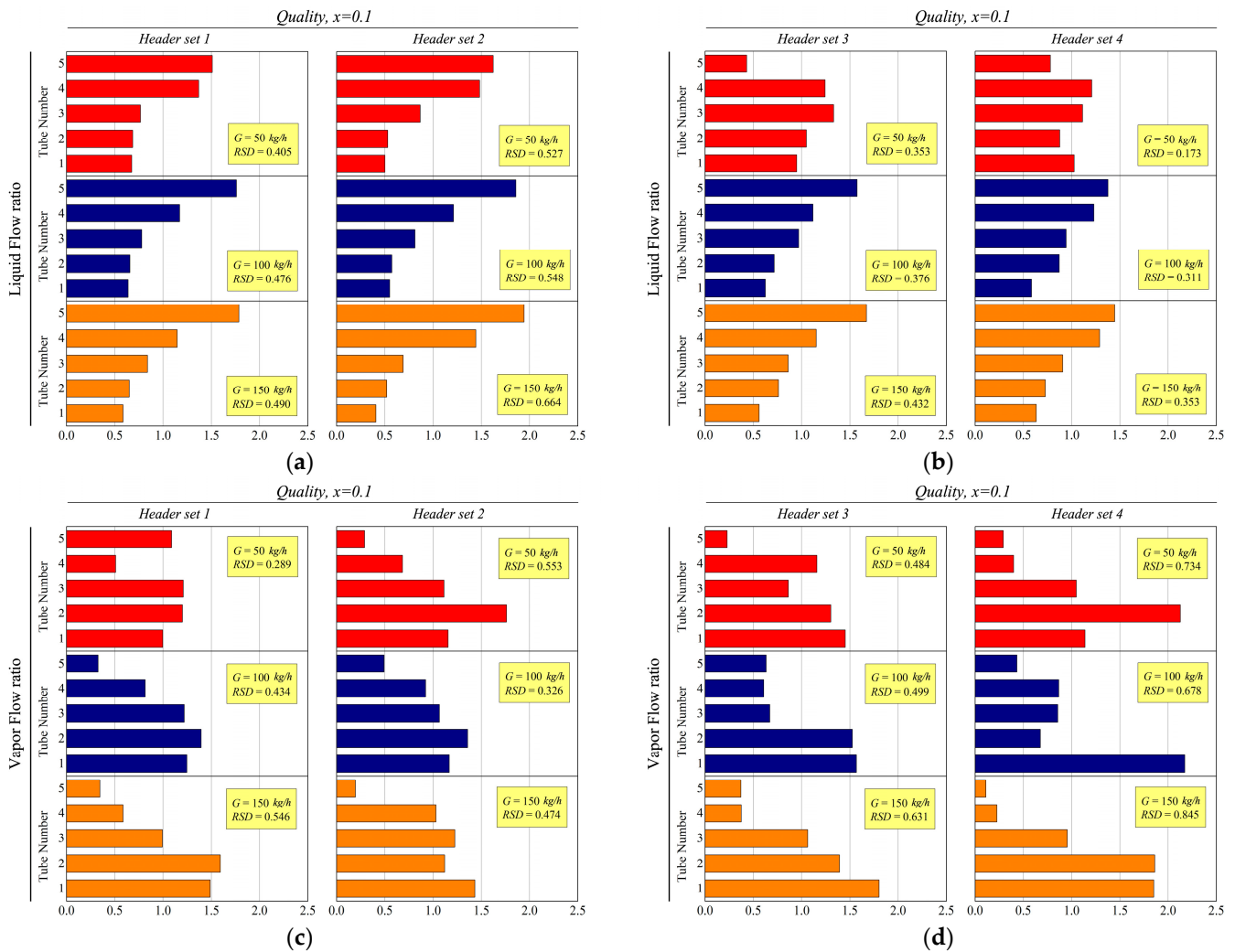


Figure 8. Effect of header outlet tube diameter to flow distribution profile: (a) liquid flow ratio, header sets 1 and 2 (190 mm); (b) liquid flow ratio, header sets 3 and 4 (490 mm); (c) vapor flow ratio, header sets 1 and 2 (190 mm); (d) vapor flow ratio, header sets 3 and 4 (490 mm).

3.3.3. Effect of Header Height

Figure 9 shows the flow distribution profiles at $x = 0.1$ according to the change in header height. The header sets with the same header outlet tube diameter set were grouped and compared. It is generally observed for all the considered inlet mass flow rates that the liquid flow ratio is lower at the upper section in the tall header as compared with the short header. Moreover, the tall header exhibits a lower RSD for the liquid flows. This means that while an excessive inertial force is demonstrated in the short header (190 mm), it is relatively moderate in the tall header (490 mm). In particular, despite the lower inlet mass flow rate (50 kg h^{-1}), a large amount of liquid flows at the upper portion of the header set 2 due to a large outlet tube diameter in this section. However, as the height increases, the excessive liquid influx to the upper section is relieved, and a relatively well-distributed liquid flow is obtained, as in the case of header set 4.

On the other hand, for the vapor flow ratio, RSD tends to increase as the inflow to the upper section decreases when the height of the header increases. This result is due to the vapor flow decrement as the liquid flow ratio to the upper section decreases.

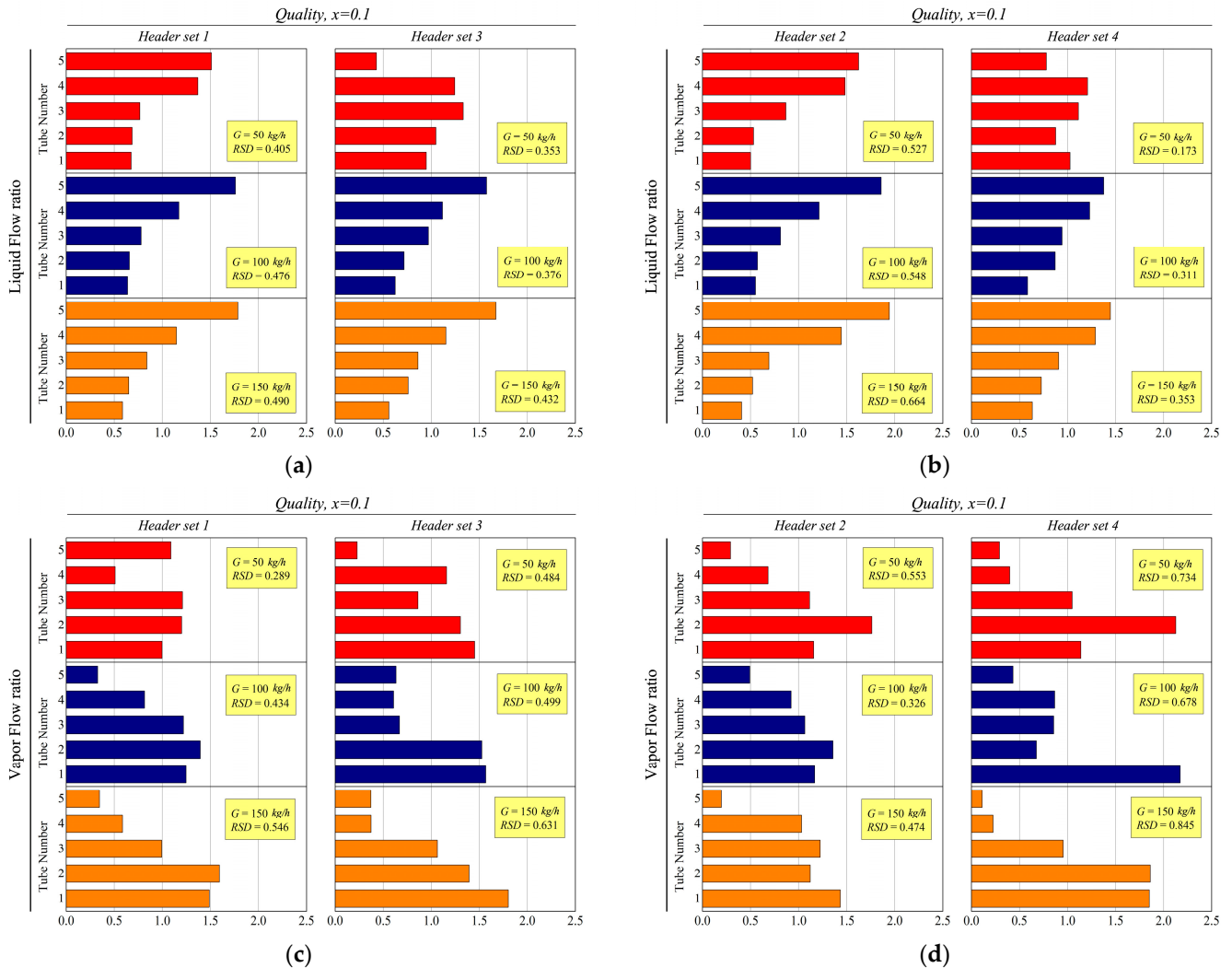


Figure 9. Effect of header height to flow distribution profile: (a) liquid flow ratio, header sets 1 and 3 (190 mm and 490 mm); (b) liquid flow ratio, header sets 2 and 4 (190 mm and 490 mm); (c) vapor flow ratio, header sets 1 and 3 (190 mm and 490 mm); (d) vapor flow ratio, header sets 2 and 4 (190 mm and 490 mm).

3.4. Dimensionless Number Analysis

As described above, the flow distribution in the vertical header is a result of various physical interactions such as inertial force, viscous force, and gravitational force. To understand the previous observation results, the Reynolds and Froude numbers of the flow inside the vertical header can be considered. The two-phase flow distribution notation in the header and each tube is defined in Figure 10.

To comprehensively evaluate the effects of the parameters considered in this study, this section presents investigation results regarding the effects of the flow rate, inlet vapor quality, and header sets based on the dimensionless number of a two-phase mixture. The Reynolds and Froude numbers for the two-phase mixture are expressed in Equations (9) and (10), respectively.

$$Re_{h,tp,i} = \frac{G_{h,tp,i}D}{\mu_{h,tp,i}} \quad (9)$$

$$Fr_{h,tp,i} = \frac{G_{h,tp,i}^2}{gL_i\rho_{h,tp,i}^2} \quad (10)$$

Here, L_i is the individual characteristic length of the Froude number, defined as the height from the inlet of the header to the inlet of each branch tube.

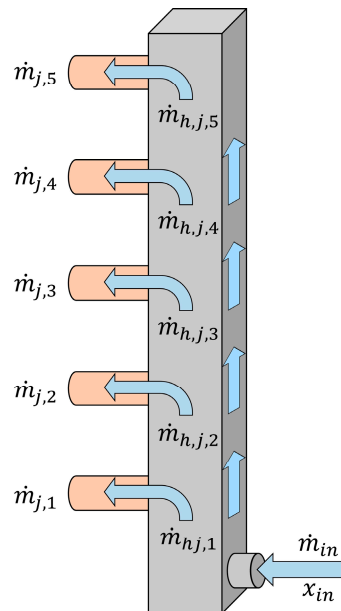


Figure 10. Flow notation in the vertical header and branching tubes.

3.4.1. Reynolds Number

Figure 11a depicts the change in the Reynolds number according to the inlet vapor quality of the header. Regardless of the inlet flow rate, the Reynolds number increases as the inlet vapor quality increases. A rise in the inlet vapor quality indicates an increase in the vapor flow rate in the vertical header. Furthermore, increasing the inlet vapor quality causes a significant increase in the void fraction. In the case when vapor quality is equal to 0.2, the void fraction is approximately 0.5–0.7. Therefore, a slight increase in the inlet vapor quality causes a relatively high volume flux, wide cross-sectional area, and high vapor-phase speed. Moreover, the high-volume flux of the vapor phase leads to an increase in the Reynolds number (increase in inertia) of the entire two-phase mixture. As a result, the amount of liquid or vapor flow to the upper region of the header increases.

Figure 11b depicts the change in the Reynolds number when the header outlet inner diameter set changes for a header height of 190 mm. Header set 2, which has a different outlet inner diameter, has a higher Reynolds number compared with header set 1, with a fixed outlet inner diameter regardless of the inlet flow rate. As previously described, the large outlet inner diameter gradually expands from the bottom (tube number 1, 2.2 mm) to the top (tube number 5, 3.2 mm). Accordingly, the resistance of the flow distribution decreases, and the Reynolds number consequently increases. However, it can be observed that the change in the outlet inner diameter causes an effective change only at a flow rate of 150 kg h^{-1} , where the effect is concentrated in tube numbers 3 and 4. These observations are evident from the liquid and vapor flow ratio results depicted in Figures 5 and 6. It can be understood that the flow distribution can be controlled by changing the outlet diameter of the vertical header.

Figure 11c illustrates the effect of the vertical header height variation on the Reynolds number. The Reynolds number is generally lower at header set 3 (490 mm height) compared with that of header set 1 (190 mm height) for all the considered flow rates. The flow is concentrated at the bottom part of the header due to lesser resistances in the taller header, which also indicates lesser inertial forces or Reynolds number. The liquid and vapor

flow ratios in the upper tubes decrease along with an increase in the header height. As the gravitational force becomes more dominant, the consideration of the Froude number becomes significant.

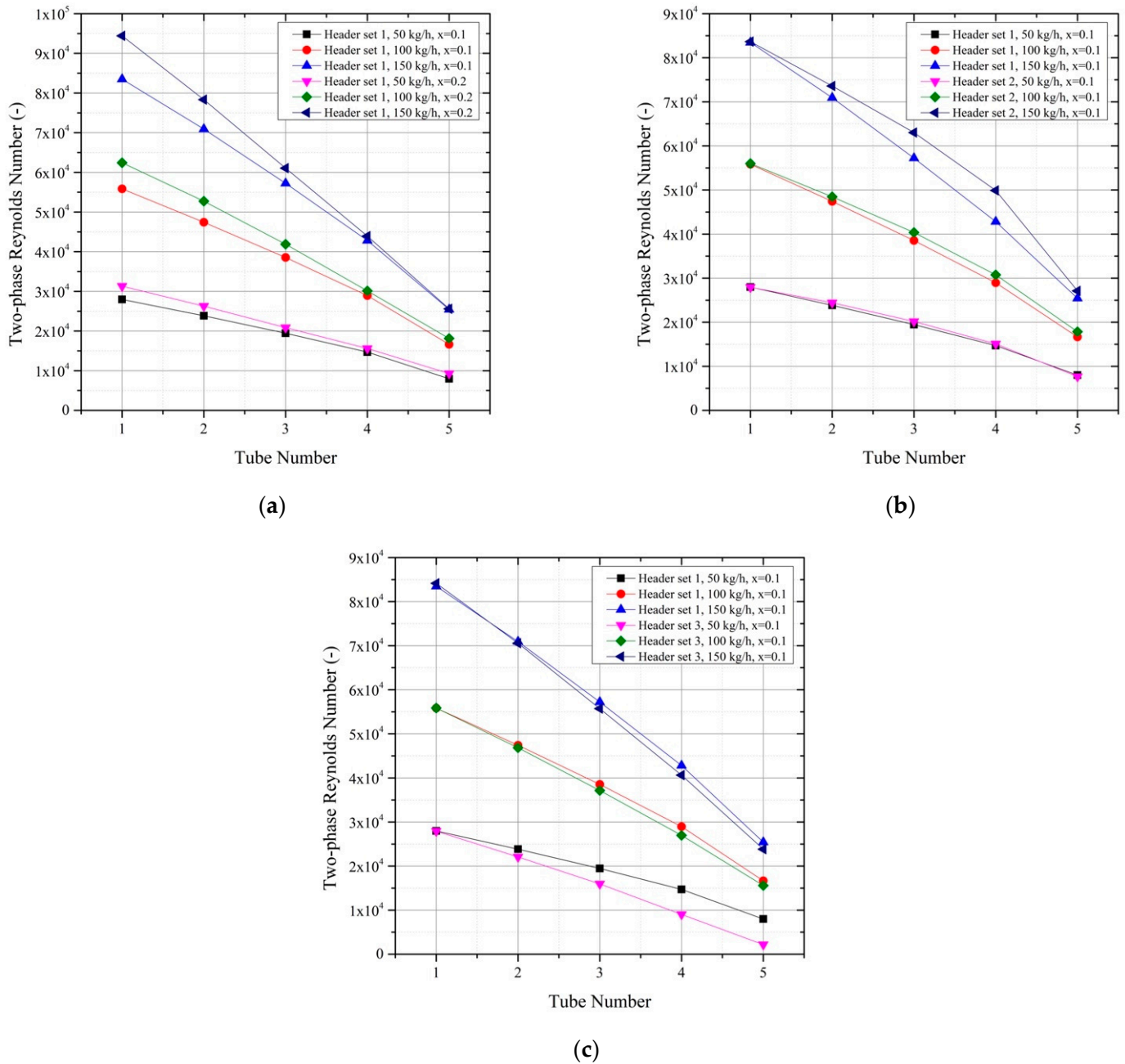


Figure 11. Reynolds number according to the experimental parameters: (a) inlet vapor quality variation; (b) header outlet diameter variation; (c) header height variation.

3.4.2. Froude Number

Figure 12a depicts the variation in Froude numbers inside the 190 mm vertical header according to the inlet vapor quality variation. For all the flow rates, the Froude number increases as the inlet quality increases. Similar to the trends of the Reynolds number, the inlet vapor quality leads to an increase in the inertial force of the entire two-phase mixture, and it shows an increasing Froude number. As a result, the increased inertial force compared to the height effect (gravity) increases the flow amount of the traversing liquid and vapor towards the top tubes.

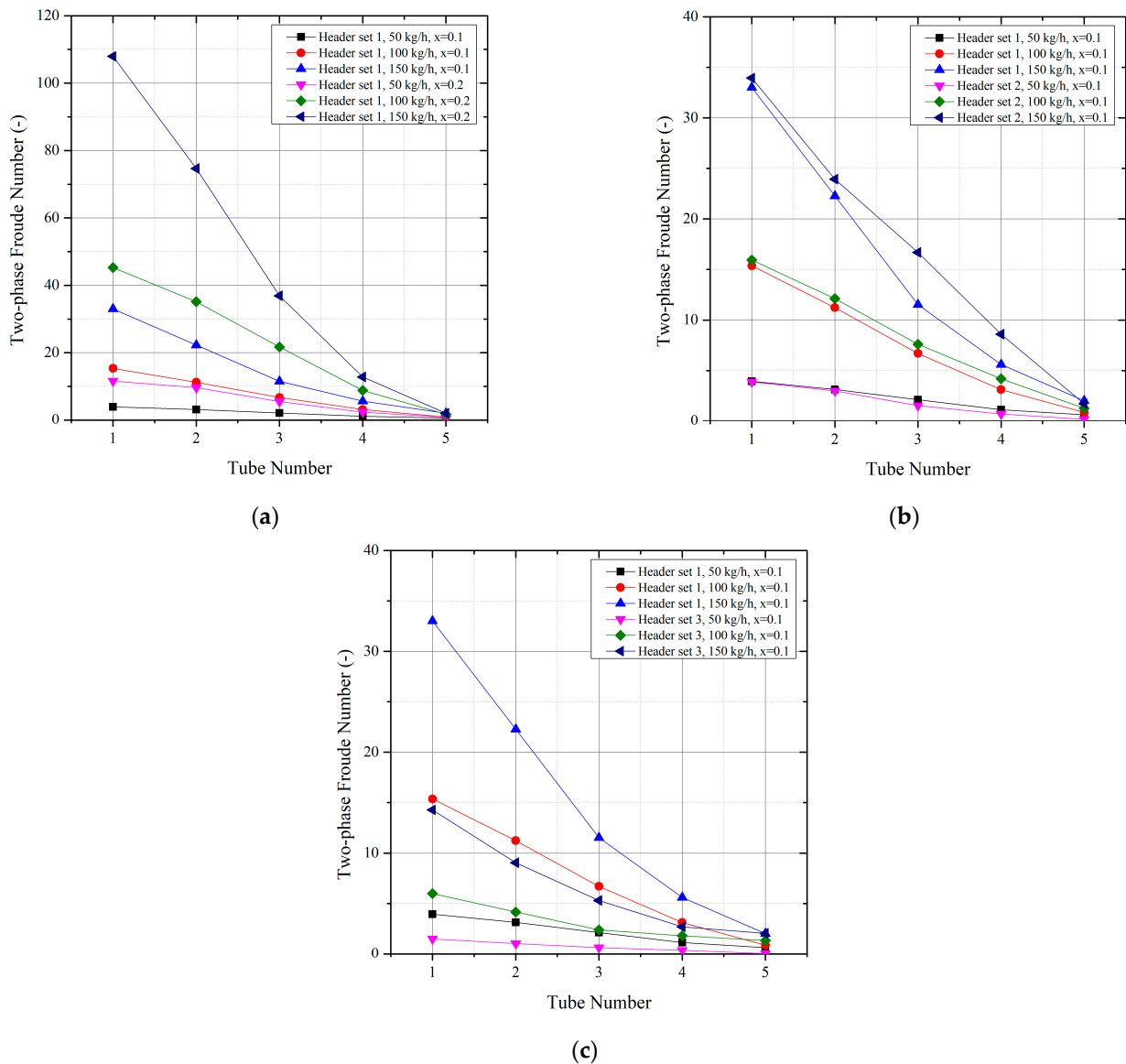


Figure 12. Froude number according to the experimental parameters: (a) inlet vapor quality variation; (b) header outlet diameter variation; (c) header height variation.

Figure 12b shows the variation in the Froude number according to the large diameter in the upper tube section of the vertical header with a height of 190 mm. Regardless of the flow rate, the different outlet inner diameter set of the header (header set 2) leads to increased inertia compared to the case of the same outlet inner diameter (header set 1). That is, the Froude number is higher in the header set 2. Therefore, the liquid/vapor phase amount to the upper section (towards tube number 5) increases even with the same header inlet quality.

Figure 12c depicts the effect of the height variation on the Froude numbers inside the vertical header. As hypothesized, owing to an increase in the local gravity due to the individual height increment from the header inlet, the Froude number consequently decreases. Thus, the height adjustment can modulate the excessive liquid flow exiting at the top branch tubes in the 190 mm header observed in Figure 4.

3.5. Flow Distribution Correlation

In this section, the flow distribution correlation that can predict the flow distribution in the vertical header is derived from measured experimental results. However, it should

be noted that the flow distribution prediction described in this chapter is an empirical result of specific headers considered in this study. Hence, its application to vertical headers with different structures may exhibit limitations.

The flow distribution in the vertical header can be expressed and described using the Reynolds number, Froude number, dimensionless numbers of inertia, viscosity, and gravity, as previously shown. In particular, the prediction of the flow distribution of the liquid phase is of interest from the perspective of evaporator heat exchanger design to prevent dry-out in the branching tubes. Watanabe et al. [31] introduced the liquid distribution ratio ($\dot{m}_{l,i} / \dot{m}_{h,l,i}$), which is the liquid taken off at the local tube to the liquid at the immediate header, and the distribution notation is shown in Figure 7. Watanabe et al. [31], Byun and Kim [32], Zou and Hrnjak [33,34], and Redo et al. [24] proposed various empirical correlations using the Reynolds or Froude numbers to predict the liquid distribution ratio. Table 3 summarizes the conditions and empirical correlations suggested in the previous studies.

Table 3. Conditions and empirical correlation of previous studies.

Authors	Working Fluid	\dot{m}_{in} (kg h ⁻¹)	G_{in} (kg m ⁻² s ⁻¹)	x_{in}	T_{sat} (°C)	Protrusion (%)	Correlation
Watanabe et al.	R11	45–135	40–120	0–0.4	-	0	$\frac{\dot{m}_{l,i}}{\dot{m}_{h,l,i}} = 2.74e^{-5} Re_v - 0.0124 Re_v^{0.5} + 1.37$
Byun and Kim	R410A	46–64	50–70	0.3	5	50	$\frac{\dot{m}_{l,i}}{\dot{m}_{h,l,i}} = 6.98 Re_v^{-0.42}$
Zou and Hrnjak (i)	R134a	15–45	17.95–52.4	0.2–0.8	10	50, 75	$\frac{\dot{m}_{l,i}}{\dot{m}_{h,l,i}} = 39389 x_{in}^{1.122} \left(\frac{A_{min}}{A}\right)^{0.355} Re_v^{-1.153}$
Zou and Hrnjak (ii)	R410A	15–45	17.95–52.4	0.2–0.8	5	50	$\frac{\dot{m}_{l,i}}{\dot{m}_{h,l,i}} = 421989 x_{in}^{1.248} Re_v^{-1.447}$
M. A. Redo et al.	R410a	40–200	50–250	0.1–0.6	10, 15	0, 50	$\frac{\dot{m}_{l,i}}{\dot{m}_{h,l,i}} = 0.131 x_{in}^{-0.1} Fr_l^{-0.373}$

The above empirical correlations for the liquid distribution ratio are shown for the measurement results. All correlation equations are similar to the actual (experimental) liquid flow ratio in Figure 13. Among them, the correlation equation of Redo et al. was found to be relatively consistent with the measurement results, while most correlation equations did not sufficiently predict the experimental results.

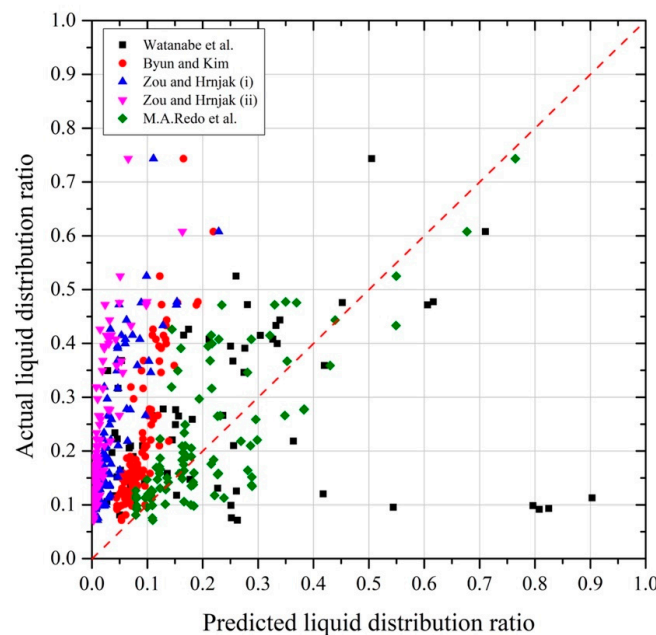


Figure 13. Previous correlations [24,31–34] vs. actual liquid distribution ratio.

As described in the study of Redo et al. [24], there are differences between the proposed correlations owing to the target experimental applications, which are related to the physical configurations of the header and the operating conditions. The present study has investigated the flow distribution considering the header height, header outlet inner diameter, inlet flow rate, and inlet vapor quality as parameters that differ from the previous studies. In particular, a mass flux of 908–2723 kg m⁻² s⁻¹ was considered, which is very high compared to the considerations of the existing studies [24,29–32]. Therefore, it is necessary to establish a new empirical correlation that satisfies the corresponding conditions.

The inlet vapor quality (x_{in}), liquid-phase Reynolds number ($Re_{h,l,i}$), and liquid-phase Froude number ($Fr_{h,l,i}$) were considered to investigate the effect of each parameter on the liquid distribution ratio in this study. Here, the Reynolds and Froude numbers of the liquid phase are expressed in Equations (11) and (12), respectively.

$$Re_{h,l,i} = \frac{G_{h,l,i}D}{\mu_{h,l,i}} \quad (11)$$

$$Fr_{h,l,i} = \frac{G_{h,l,i}^2}{gL_i\rho_{h,l,i}^2} \quad (12)$$

From this, a generalized expression is constructed as in Equation (13), and the coefficients in which the expression represents the maximum coefficient of determination (R-square) are $C_1 = 7.6 \times 10^{-6}$, $C_2 = -0.4$, $C_3 = 0.89$, $C_4 = -0.615$.

$$\frac{\dot{m}_{l,i}}{\dot{m}_{h,l,i}} = C_1 x_{in}^{C_2} Re_{h,l,i}^{C_3} Fr_{h,l,i}^{C_4} \quad (13)$$

The predicted versus actual liquid distribution ratio graph of the correlation proposed in this study is depicted in Figure 14. The R-squared value was 0.76, predicted to be $\pm 30\%$ deviation in most ranges.

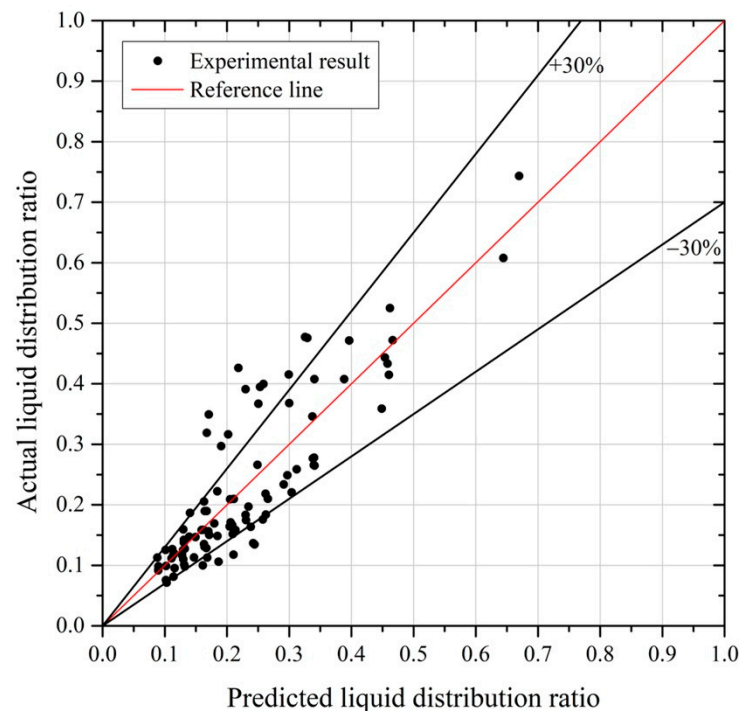


Figure 14. Predicted vs. actual liquid distribution ratio.

The proposed correlation provides a relatively accurate prediction of the two-phase flow distribution within the vertical header tested in this study. This can be applied to

similar vertical headers for air-conditioning applications operating in a similar range of conditions. However, because this correlation is aimed at a practical case, there might be a limitation in applying it to a vertical header with a different structure from that of the headers being considered in this study.

4. Conclusions

This study aimed to investigate the flow distribution characteristics of a vertical header, which functions as an evaporator of a heat pump system with an R410A as the working fluid. The considered vertical headers with a reduced cross-sectional area have a high mass flux and are characterized by high Reynolds numbers compared to the previously reported vertical headers. The flow distribution was analyzed by considering the following parameters: vertical header height, branch pipe diameter, inlet flow rate, and inlet quality. Generally, it is recommended for a practical design that the average Froude number in the header be kept as small as possible, and the liquid Reynolds number at the inlet of the header be maintained as high as possible to avoid extreme flow maldistribution (dry-out). Specifically, the following conclusions are drawn:

1. The vertical headers considered in the study exhibit high Reynolds number, where the liquid flow is concentrated at the top and the vapor flow at the bottom sections. This characteristic causes the concentration of the liquid flow ratio to deteriorate in the upper section of the vertical header, and the concentration of the vapor flow ratio is moderated in the lower section. These trends were exhibited in most of the experimental conditions, particularly for the 190 mm header.
2. The flow distribution results were confirmed more intuitively using the relative standard deviation (RSD). The smaller the RSD value, the more uniform the flow distribution becomes. In the case of the liquid phase, the minimum value of RSD in the header set 4 (490 mm header, different outlet inner diameters) was 0.17. For the vapor phase, the header set 2 (190 mm header, different outlet inner diameters) had a minimum RSD value of 0.18.
3. The flow distribution characteristics of the vertical header were analyzed using Reynolds and Froude numbers, which are dimensionless numbers of inertia, viscosity, and gravity. To predict the liquid distribution ratio ($\dot{m}_{l,i} / \dot{m}_{h,l,i}$), as the available correlations in the literature have compromised prediction accuracy, we proposed a new empirical correlation that considers the liquid-phase Reynolds and Froude numbers. The derived correlation could predict the liquid distribution ratio within $\pm 30\%$.

The results of this study confirmed that the feasibility of the rational flow distribution could be derived according to the header's physical configuration (cross-sectional area, height, outlet inner diameter) and operating conditions (flow rate, quality, and temperature). It is also expected that the flow distribution can be controlled by combining these parameters. However, the study of a vertical header, which was designed for practical cases, shows the limitations of the application and expansion of results. For this, a systematic establishment and analysis of the vertical header's general design parameters and operating conditions are recommended. In addition, the rational flow distribution in the vertical header can be extended to consider its effect on the efficiency and capacity of vapor compression refrigeration systems in the future. For instance, an increase in the Reynolds number in the evaporator header causes a large pressure drop, which leads to a decrease in overall system performance. Such interrelationship across hydrodynamics, heat transfer, and thermodynamics will be carried out as a follow-up study.

Author Contributions: Conceptualization, S.L. and H.K.; methodology, M.K. and M.A.R.; validation, M.K., M.A.R. and J.J.; formal analysis, M.K.; investigation, M.K. and M.A.R.; resources, K.S.; data curation, M.K.; writing—original draft preparation, M.K.; writing—review and editing, M.A.R., J.J., K.S., S.L. and H.K.; supervision, J.J. and K.S.; project administration, K.S.; funding acquisition, K.S. All authors have read and agreed to the published version of the manuscript.

Funding: This article is based on results obtained from a project, JPNPP18005, commissioned by the New Energy and Industrial Technology Development Organization (NEDO).

Data Availability Statement: Not applicable.

Conflicts of Interest: The authors declare no conflict of interest.

References

1. Shen, B.; Fricke, B. Development of High Efficiency Window Air Conditioner Using Propane under Limited Charge. *Appl. Eng.* **2020**, *166*, 114662. [[CrossRef](#)]
2. Illán-Gómez, F.; García-Cascales, J.R.; Hidalgo-Mompeán, F.; López-Belchí, A. Experimental Assessment of the Replacement of a Conventional Fin-and-Tube Condenser by a Minichannel Heat Exchanger in an Air/Water Chiller for Residential Air Conditioning. *Energy Build* **2017**, *144*, 104–116. [[CrossRef](#)]
3. Cho, H.; Cho, K. Mass flow rate distribution and phase separation of R-22 in multi-microchannel tubes under adiabatic condition. *Microscale Thermophys. Eng.* **2004**, *8*, 129–139. [[CrossRef](#)]
4. Prakash, S.; Kumar, S. Fabrication of Rectangular Cross-Sectional Microchannels on PMMA with a CO₂ Laser and Underwater Fabricated Copper Mask. *Opt. Laser Technol.* **2017**, *94*, 180–192. [[CrossRef](#)]
5. Nguyen, T.Q.; Park, W.-T. Rapid, Low-Cost Fabrication of Circular Microchannels by Air Expansion into Partially Cured Polymer. *Sens. Actuators B Chem.* **2016**, *235*, 302–308. [[CrossRef](#)]
6. Botticella, F.; de Rossi, F.; Mauro, A.W.; Vanoli, G.P.; Viscito, L. Multi-Criteria (Thermodynamic, Economic and Environmental) Analysis of Possible Design Options for Residential Heating Split Systems Working with Low GWP Refrigerants. *Int. J. Refrig.* **2018**, *87*, 131–153. [[CrossRef](#)]
7. Han, Y.; Liu, Y.; Li, M.; Huang, J. A Review of Development of Micro-Channel Heat Exchanger Applied in Air-Conditioning System. *Energy Procedia* **2012**, *14*, 148–153. [[CrossRef](#)]
8. Panghat, K.; Mehendale, S.S.; Mehendale, S. A Critical Assessment of Two-Phase Flow Distribution in Microchannel Heat Exchangers. In Proceedings of the International Refrigeration and Air Conditioning Conference, West Lafayette, IN, USA, 11–14 July 2016.
9. Boteler, L.; Jankowski, N.; McCluskey, P.; Morgan, B. Numerical Investigation and Sensitivity Analysis of Manifold Microchannel Coolers. *Int. J. Heat Mass Transf.* **2012**, *55*, 7698–7708. [[CrossRef](#)]
10. Kulkarni, T.; Bullard, C.W.; Cho, K. Header Design Tradeoffs in Microchannel Evaporators. *Appl. Eng.* **2004**, *24*, 759–776. [[CrossRef](#)]
11. Saha, S.K.; Celata, G.P. *Instability in Flow Boiling in Microchannels*; Springer: Berlin/Heidelberg, Germany, 2015.
12. Wu, Z.; Li, W. A New Predictive Tool for Saturated Critical Heat Flux in Micro/Mini-Channels: Effect of the Heated Length-to-Diameter Ratio. *Int. J. Heat Mass Transf.* **2011**, *54*, 2880–2889. [[CrossRef](#)]
13. Mastrullo, R.; Mauro, A.W.; Viscito, L. Experimental CHF for Low-GWP Fluids and R134a. Effect of the Lh/D Ratio at Low and High Mass Velocities. *Int. J. Heat Mass Transf.* **2017**, *109*, 1200–1216. [[CrossRef](#)]
14. Mastrullo, R.; Mauro, A.W.; Thome, J.R.; Vanoli, G.P.; Viscito, L. Critical Heat Flux: Performance of R1234yf, R1234ze and R134a in an Aluminum Multi-Minichannel Heat Sink at High Saturation Temperatures. *Int. J. Therm. Sci.* **2016**, *106*, 1–17. [[CrossRef](#)]
15. Amador, C.; Gavriilidis, A.; Angeli, P. Flow Distribution in Different Microreactor Scale-out Geometries and the Effect of Manufacturing Tolerances and Channel Blockage. *Chem. Eng. J.* **2004**, *101*, 379–390. [[CrossRef](#)]
16. Kandlikar, S.G.; Lu, Z.; Domigan, W.E.; White, A.D.; Benedict, M.W. Measurement of Flow Maldistribution in Parallel Channels and Its Application to Ex-Situ and in-Situ Experiments in PEMFC Water Management Studies. *Int. J. Heat Mass Transf.* **2009**, *52*, 1741–1752. [[CrossRef](#)]
17. Cho, E.S.; Choi, J.W.; Yoon, J.S.; Kim, M.S. Modeling and Simulation on the Mass Flow Distribution in Microchannel Heat Sinks with Non-Uniform Heat Flux Conditions. *Int. J. Heat Mass Transf.* **2010**, *53*, 1341–1348. [[CrossRef](#)]
18. Mueller, A.C.; Chiou, J.P. Review of Various Types of Flow Maldistribution in Heat Exchangers. *Heat Transf. Eng.* **1988**, *9*, 36–50. [[CrossRef](#)]
19. Kitto, J.B.; Robertson, J.M. Effects of Maldistribution of Flow on Heat Transfer Equipment Performance. *Heat Transf. Eng.* **1989**, *10*, 18–25. [[CrossRef](#)]
20. Dario, E.R.; Tadrist, L.; Passos, J.C. Review on Two-Phase Flow Distribution in Parallel Channels with Macro and Micro Hydraulic Diameters: Main Results, Analyses, Trends. *Appl. Eng.* **2013**, *59*, 316–335. [[CrossRef](#)]
21. Siddiqui, O.K.; Zubair, S.M. Efficient Energy Utilization through Proper Design of Microchannel Heat Exchanger Manifolds: A Comprehensive Review. *Renew. Sustain. Energy Rev.* **2017**, *74*, 969–1002. [[CrossRef](#)]
22. Lee, J.K. Two-Phase Flow Behavior inside a Header Connected to Multiple Parallel Channels. *Exp. Fluid Sci.* **2009**, *33*, 195–202. [[CrossRef](#)]
23. Hwang, Y.; Jin, D.-H.; Radermacher, R. Refrigerant Distribution in Minichannel Evaporator Manifolds. *HVACR Res.* **2007**, *13*, 543–555. [[CrossRef](#)]
24. Redo, M.A.; Jeong, J.; Giannetti, N.; Enoki, K.; Yamaguchi, S.; Saito, K.; Kim, H. Characterization of Two-Phase Flow Distribution in Microchannel Heat Exchanger Header for Air-Conditioning System. *Exp. Fluid Sci.* **2019**, *106*, 183–193. [[CrossRef](#)]

25. Fei, P.; Hrnjak, P.S. *Adiabatic Developing Two-Phase Refrigerant Flow in Manifolds of Heat Exchangers*; University of Illinois at Urbana-Champaign: Champaign, IL, USA, 2004; Volume 61801.
26. Ahmad, M.; Berthoud, G.; Mercier, P. General Characteristics of Two-Phase Flow Distribution in a Compact Heat Exchanger. *Int. J. Heat Mass Transf.* **2009**, *52*, 442–450. [[CrossRef](#)]
27. Liu, Y.; Sun, W.; Wu, W.; Wang, S. Gas-Liquid Two-Phase Flow Distribution in Parallel Micro-Channels with Different Header and Channels' Orientations. *Int. J. Heat Mass Transf.* **2017**, *112*, 767–778. [[CrossRef](#)]
28. Nielsen, K.K.; Engelbrecht, K.; Christensen, D.V.; Jensen, J.B.; Smith, A.; Bahl, C.R.H. Degradation of the Performance of Microchannel Heat Exchangers Due to Flow Maldistribution. *Appl. Eng.* **2012**, *40*, 236–247. [[CrossRef](#)]
29. Zhu, Q.; Pishahang, M.; Bichnevicius, M.; Amy, C.; Caccia, M.; Sandhage, K.H.; Henry, A. The Importance of Maldistribution Matching for Thermal Performance of Compact Heat Exchangers. *Appl. Energy* **2022**, *324*, 119576. [[CrossRef](#)]
30. Brown, C.E. *Applied Multivariate Statistics in Geohydrology and Related Sciences*; Springer: Berlin/Heidelberg, Germany, 1998; ISBN 978-3-642-80330-7.
31. Watanabe, M.; Katsuta, M.; Nagata, K. Two-Phase Flow Distribution in Multi-Pass Tube Modeling Serpentine Type Evaporator. *ASME/JSME Therm. Eng. Conf.* **1995**, *2*, 35–42.
32. Byun, H.W.; Kim, N.H. Refrigerant Distribution in a Parallel Flow Heat Exchanger Having Vertical Headers and Heated Horizontal Tubes. *Exp. Fluid Sci.* **2011**, *35*, 920–932. [[CrossRef](#)]
33. Zou, Y.; Hrnjak, P.S. Refrigerant Distribution in the Vertical Header of the Microchannel Heat Exchanger—Measurement and Visualization of R410A Flow. *Int. J. Refrig.* **2013**, *36*, 2196–2208. [[CrossRef](#)]
34. Zou, Y.; Hrnjak, P.S. Experiment and Visualization on R134a Upward Flow in the Vertical Header of Microchannel Heat Exchanger and Its Effect on Distribution. *Int. J. Heat Mass Transf.* **2013**, *62*, 124–134. [[CrossRef](#)]